Absorption spectra of driven degenerate two-level atomic systems

A. Lipsich, S. Barreiro, A. M. Akulshin,* and A. Lezama†
Instituto de Física, Facultad de Ingeniería, Casilla de Correo 30, 11000 Montevideo, Uruguay
(Received 17 September 1999; published 10 April 2000)

The absorption properties of *degenerate* two-level atomic systems tested by a weak probe field in the presence of an intense pump field have been analyzed. The theoretical model previously presented in Phys. Rev. A **61**, 013801 (1999) that appears to be suitable for arbitrary choices of the pump intensity, level angular momenta, and pump and probe polarizations, was used for the calculation of the spectra for several basic configurations. Experimental absorption spectra obtained on a Rb atomic beam for different pump and probe field polarizations show good agreement with the calculation. The spectra are in general essentially different from and more complex than the classical Mollow absorption triplet.

PACS number(s): 42.50.Gy, 42.50.Hz, 32.70.−n

I. INTRODUCTION

The calculation and subsequent observation of the spectroscopic properties of pure two-level systems (PTLS's) consisting of two *nondegenerate* energy levels driven by a strong monochromatic field constitute one of the classical achievements in the field of nonlinear optics. This textbook problem [1,2] presents in their simplest form the basic effects of nonlinear light-matter interaction such as power broadening, light shifts, and coherence transfer between light and atom. The absorption spectrum of a strongly driven two-level atom was first calculated by Mollow [3] and observed by Wu and co-workers [4]. This spectrum has a characteristic triplet structure (Fig. 1) to which we will refer in this paper as the Mollow absorption spectrum (MAS). The fluorescence spectrum of the driven two-level system was also calculated and observed by Mollow and collaborators [5].

An important step toward the understanding of the spectroscopic features of driven PTLS's is given by the dressed-atom model developed by Cohen-Tannoudji and collaborators [6]. This model provides a very simple and intuitive picture of the energy exchanges in the coupled atom plus drive field system.

The theory of the spectroscopic response of PTLS's has proven to be quite useful for the qualitative understanding of a large number of observations. It is nevertheless a simplification. Actual energy levels in atoms, molecules or solids are generally degenerate. Obviously, *degenerate* two-level systems (DTLS's) are more complex than PTLS's. The actual number of involved sublevels is larger and this introduces diversity in the matrix elements describing the atom-field coupling. Also, when degenerate levels are considered, the vectorial nature of the electromagnetic field is essential and manifests itself via the optical polarization dependence of the response.

In recent years several phenomena have been studied where DTLS's play an essential role. Good examples are most of the atomic trapping and cooling experiments. The well known magneto-optical neutral atom trap relies on energy level degeneracy for its operation [7]. This is also the case for sub-Doppler [8] and subrecoil atom cooling techniques [9]. Some observations made during these experiments also demonstrate the need for a deeper understanding of the spectral properties of driven DTLS's. A typical example is the observation of a narrow structure presenting absorption and gain in magneto-optically trapped atoms [10,11]. This feature could not be interpreted in the framework of a simple two-level model. It should be mentioned that in this case the atoms are driven in a cycling transition involving degenerate levels and are in the presence of a quite complicated spatial pattern of optical polarization. This narrow feature was assigned to a Raman transition between ground-state Zeeman sublevels [11]. More recently, we have shown that the level degeneracy plays an essential role in the spectroscopic response of DTLS's driven by a resonant field whose intensity is comparable with or lower than the saturation intensity [12–14].

Some attempts have been made to calculate the spectroscopic response of DTLS's. Berman and co-workers have developed a theoretical treatment based on the optical Bloch

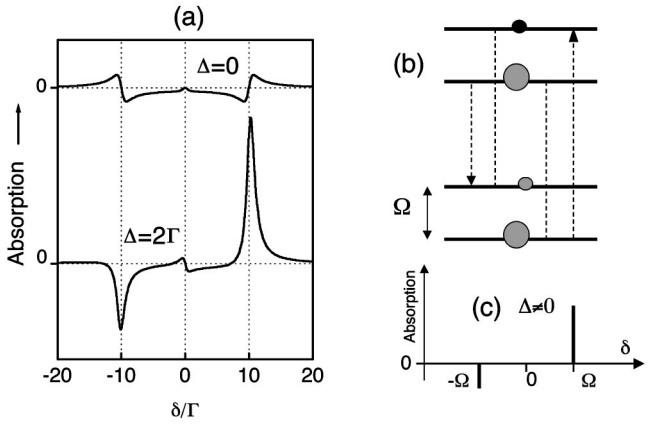

FIG. 1. Probe absorption spectra for a driven pure two-level system. (a) Calculated absorption spectra for $\Delta=0$ and $\Delta=2\Gamma$ with $\Omega_0=10\Gamma$. (b) Schematic representation of the dressed-atom (ladder) level structure. Circles represent level occupation. Arrows indicate probed transitions. (c) Structure of the absorption spectrum inferred from the dressed-atom model.

*Permanent address: Lebedev Physics Institute, 117924 Moscow, Leninsky pr. 53, Russia.
†Electronic address: alezama@fing.edu.uy

equation applied to the density matrix of the driven atomic system [15–17]. On the other hand Bo Gao has developed a model appropriate to the description of a DTLS driven by a linearly polarized field [18,19]. He demonstrated that the absorption experienced by a probe beam with polarization perpendicular to that of the pump presents similar structures to that observed in the magneto-optical trap [10,11]. Recently, we have presented a theoretical model well suited for the numerical calculation of the response of DTLS's in the general case [13,14]. This model was used for the analysis of coherence resonances arising in the two-field spectroscopy of DTLS's under weak or moderate pump field intensity.

The aim of this paper is to analyze, both theoretically and experimentally, the weak probe absorption spectra of driven atomic transitions between two degenerate atomic levels possessing well defined angular momentum and forming a closed system (no transition to other atomic levels allowed). The next section of the paper will be devoted to the presentation of the calculated absorption spectra under different assumptions for the atomic transition and optical field polarizations. In the third section, experimental observations carried out on a rubidium atomic beam are presented and discussed.

II. THEORETICAL APPROACH

Before considering the case of DTLS's let us recall the classical result concerning the absorption spectrum (MAS) of a PTLS (Fig. 1) driven by a strong pump wave. Consider a ground level g and an excited level e separated by the energy $\hbar\omega_0$. The pump and probe field frequencies are ω_1 and ω_2, respectively, with $\delta \equiv \omega_2 - \omega_1$. The excited state decays by spontaneous emission at a rate Γ. Ω_0 is the pump Rabi frequency and $\Delta \equiv \omega_0 - \omega_1$ the pump detuning. For $\Delta \neq 0$ the MAS is asymmetric with three separate features at $\delta = 0$, $\pm\Omega$ where $\Omega \equiv (\Omega_0^2 + \Delta^2)^{1/2}$. For $\Delta > 0$, the feature at $\delta = \Omega$ in Fig. 1(a) corresponds to an absorption peak. It can be associated with the direct absorption from g to e involving one probe photon. At $\delta = -\Omega$ a gain peak is observed which corresponds (to the lowest order) to a hyper-Raman process involving the absorption of two pump photons and the stimulated emission of a probe photon. Finally, the central structure around $\delta = 0$ has a dispersionlike shape presenting gain and absorption. The positions and weights of the two sidebands, as well as their sign, can be easily derived from the dressed-atom model within the secular approximation [20] [see Figs. 1(b) and 1(c)]. In this picture, the positions of the lines in the absorption spectrum correspond to the energy differences between the dressed states. The occurrence of gain or absorption is related to the sign of the population difference between dressed states. Around $\delta = 0$ the dressed-state model within the secular approximation cannot provide a description of the central dispersionlike feature [21]. When $\Delta = 0$ the absorption spectrum is a symmetric triplet. The positions of the three components correspond to the transition energies between dressed states. However, the shape of the resonances cannot be simply derived from this model. It should be noticed that all resonances in the MAS have widths that are determined by the upper state relaxation rate Γ.

Let us now consider the case of a driven DTLS. Our analysis is based on the model recently proposed for the examination of coherence resonances arising in two-field spectroscopy of DTLS's for small and moderate pump field intensity [13,14]. With this model, the equations providing the response of the atomic system to first order in the probe intensity can be solved numerically for arbitrary values of the level degeneracy, pump intensity, and pump and probe polarizations. The present paper extends our previous study into the regime of large pump intensity (Rabi frequency larger than the natural width of the transition). No modification of the model described in [14] is required. Let us recall the basic assumptions underlying this calculation. We assume that the ground level g and an excited level e have total angular momenta F_g and F_e, respectively. The reduced matrix element of the atomic dipole operator between these levels is $\mu \equiv \langle g \| D \| e \rangle$. The finite interaction time between the atoms and light is accounted for phenomenologically through the introduction of a relaxation rate γ ensuring the return of the system to thermal equilibrium in the absence of the optical fields ($\gamma \ll \Gamma$). Since no relaxation mechanism is specifically considered for level g, γ effectively plays the role of a ground-state relaxation rate. The pump field intensity is characterized by the reduced Rabi frequency $\Omega_1 \equiv E_1 \mu/\hbar$ (E_1 is the pump field amplitude). The probe field intensity is assumed to be vanishingly small. Although this is not required by the model, in this paper we restrict ourselves to the case of closed transitions (level e decays only into level g), integer total angular momentum, and no magnetic field. The effect of collisions is not considered.

Before detailed discussion of the calculated absorption spectra, let us consider the predictions that can be made about these spectra from an elementary perspective based on optical pumping and dressed-state considerations in the limit of perfect optical pumping (strong pumping field, unlimited interaction time). We consider as an example the basic polarization schemes that will be later examined in more detail with the help of the theoretical model: pump and probe polarizations linear and parallel (ll), linear and perpendicular (lpl), circular and equal (cc), and circular and opposite (coc).

Two cases must be distinguished: (i) transitions $F_g = F \rightarrow F_e = F, F-1$ (Fig. 2) and (ii) transitions $F_g = F \rightarrow F_e = F+1$ (Fig. 3). In case (i), the optical pumping by the pump field is responsible for the accumulation of the atomic population in one or two ground-state sublevels uncoupled to the pump field (dark states). This situation greatly simplifies the atomic response. In case (ii) all ground-state sublevels are coupled to the pump field. Also, for linear pump polarization, the atomic population is distributed among all ground-state sublevels.

In case (i), when the pump and probe polarizations are the same (ll or cc), the probe absorption vanishes since all population is removed from the sublevels coupled by the light fields (this trivial situation is not illustrated in the figures). Figure 2 shows the levels and field schemes when the two polarizations are different (coc and lpl schemes) for the transitions $F_g = 2 \rightarrow F_e = 1$ and $F_g = 2 \rightarrow F_e = 2$. For simplicity,

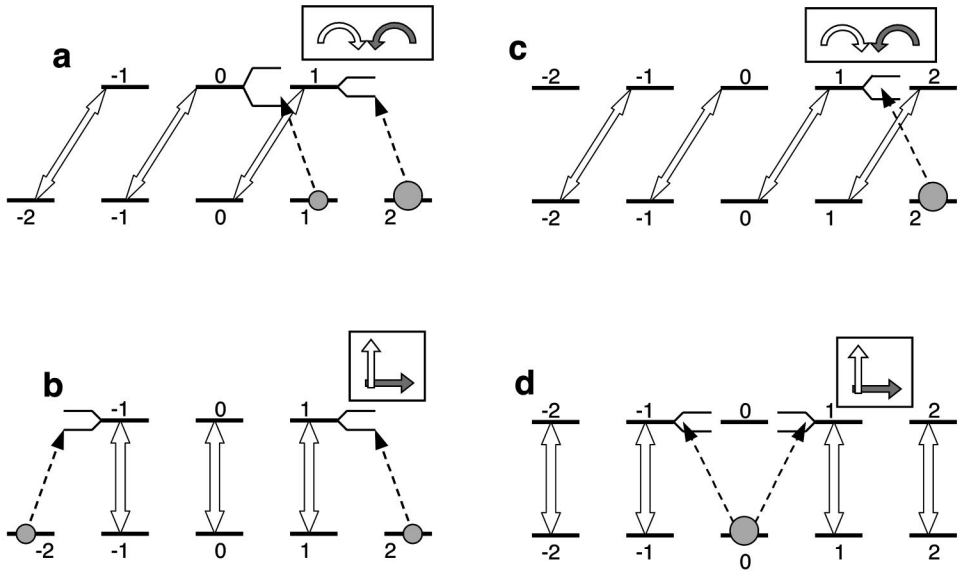

FIG. 2. Level structure for the strongly driven transitions $F_g=2\rightarrow F_e=1$ (a,b) and $F_g=2\rightarrow F_e=2$ (c,d). Circles represent level occupation. White arrows represent the pump field. Dashed arrows represent the probe field indicated only when coupled to populated levels. The ac Stark splitting due to the pump is indicated only for relevant sublevels. The pump and probe polarizations are circular and opposite (a,c) and linear and perpendicular (b,d).

the probe field (dashed) is indicated only when coupled to populated sublevels. Also the ac Stark splitting produced by the pump field on a given sublevel is represented only when it plays a role in the probe absorption. From Fig. 2 one can predict the main features of the probe absorption spectrum. It is composed of four absorption peaks in the case of a transition $F_g=F\rightarrow F_e=F-1$ with coc polarization and composed of two absorption peaks (Autler-Townes doublets) in the other three cases presented. One should notice that the results concerning the number of peaks are independent of F (provided that $F_e>0$).

In case (ii) ($F_g=1\rightarrow F_e=2$), for cc polarizations [Fig. 3(a)] the configuration reduces to a pure two-level system in which case the absorption spectrum is composed of one MAS [22]. The scheme presented in Fig. 3(b) corresponds to ll polarizations. In this case the level configuration consists of $(2F+1)$ separate two-level systems (connected through spontaneous emission). Taking into account the $m\leftrightarrow -m$ symmetry in the absence of a magnetic field (m is the ground-state magnetic quantum number), the absorption spectrum consists of $(F+1)$ MAS's sharing a common central feature at $\delta=0$. The coc polarization case is represented in Fig. 3(c). The spectrum consist of four absorption peaks corresponding to all possible transitions between two ac Stark split sublevels. Finally, the lpl polarization case is both the most complex and the most interesting. Taking into account all symmetries, the absorption spectrum is composed of $(4F+2)$ lines. However, unlike all the previously considered cases, the sign of the corresponding peaks cannot be easily predicted since competition between absorption and

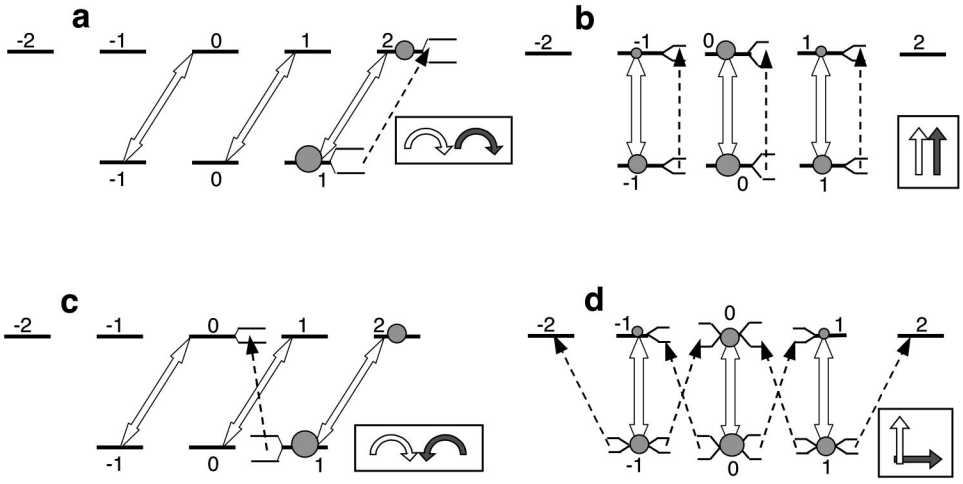

FIG. 3. Level structure for the strongly driven transition $F_g=1\rightarrow F_e=2$. Same notation as in Fig. 2. The pump and probe polarizations are circular and equal (a), linear and parallel (b), circular and opposite (c), and linear and perpendicular (d).

TABLE I. Number and nature of the spectral features in the probe absorption spectra of strongly driven degenerate two-level atoms for different atomic transitions and pump and probe polarizations linear and parallel (ll), linear and perpenicular (lpl), circular and equal (cc), and circular and opposite (coc). *A* is an absorption peak, MAS a Mollow absorption spectrum, and *P* an absorption or gain peak.

	cc	ll	coc	lpl
$F \rightarrow F-1$	0	0	$4A$	$2A$
$F \rightarrow F$	0	0	$2A$	$2A$
$F \rightarrow F+1$	1 MAS	$(F+1)$MAS	$4A$	$(4F+2)P$

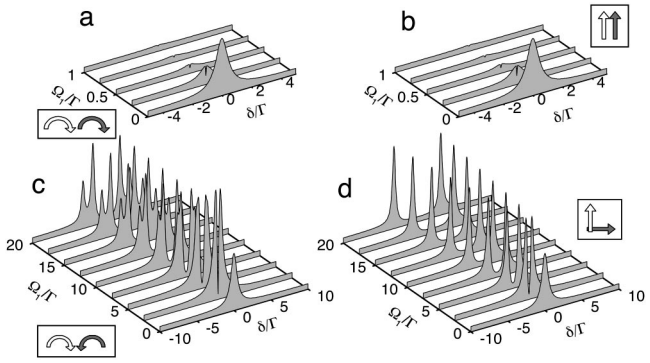

FIG. 4. Calculated probe absorption spectra for the transition $F_g=2 \rightarrow F_e=1$ as a function of the probe frequency offset δ for different values of Ω_1 and $\Delta=0$. The vertical axis corresponds to absorption. The scale (linear) is the same for all curves. The zero absorption level is given by the vertical offset common to all plots. The front plot of each series ($\Omega_1=0$) represents the linear absorption. Pump and probe polarizations are circular and equal (a), linear and parallel (b), circular and opposite (c), and linear and perpendicular (d).

gain occurs in some lines. This point will be discussed in more detail below and in the Appendix.

The results concerning the number and nature of the features present in the absorption spectra of strongly driven DTLS's with integer angular momenta are summarized in Table I. Table II presents the values of the probe to pump frequency offset δ corresponding to the positions of the probe absorption resonances as can be deduced after calculation of the positions of the ac Stark split sublevels [20].

We will discuss now the numerically calculated absorption spectra for a homogeneous ensemble of motionless atoms. Three different cases will be distinguished corresponding to $F_e-F_g=0,\pm 1$. As before we will take as representative examples the transitions $F_g=2 \rightarrow F_e=1$, $F_g=2 \rightarrow F_e=2$, and $F_g=1 \rightarrow F_e=2$.

The calculated absorption spectra for the transition $F_g=2 \rightarrow F_e=1$ are shown in Figs. 4 and 5 for $\Delta=0$ and $\Delta=2\Gamma$, respectively, as a function of the pump to probe frequency offset δ for different values of the reduced Rabi frequency Ω_1. The vertical scale (absorption) is the same for all plots. When the pump and probe polarizations are equal, the absorption decreases rapidly as Ω_1 approaches Γ, as a consequence of the optical pumping into the ground sublevels not affected by the light (dark states). Nevertheless, for $\Omega_1 \lesssim \Gamma$ a narrow dip is present in the absorption around $\delta=0$. This dip is clearly visible in Figs. 4(a,b) ($\Delta=0$) and it also exists in the cases presented in Figs. 5(a,b) ($\Delta=2\Gamma$) with a much smaller amplitude. For low pump intensities the width of this resonance is determined by γ. The origin of the narrow transparency resonance is the same as that of the narrow structure predicted for open transitions in the case of a PTLS [23–25]. It is due to the nonconservation of the total population in the ensemble of sublevels coupled to the light fields [16,17] as a consequence of the spontaneous decay into dark states. If the pump and probe polarizations are orthogonal [Figs. 4(c,d) and 5(c,d)], the optical pumping of the atomic population into ground-state Zeeman sublevels explored by the probe results in an increase of the total probe absorption with respect to linear absorption. For $\Delta=0$ [Figs. 4(c,d)] and $\Omega_1 \lesssim \Gamma$ the absorption presents at $\delta=0$ a dip of large contrast and width smaller than Γ (it is given by 2γ in the limit of weak pump intensity). This dip corresponds to electromagnetically induced transparency (EIT) in the Λ configurations formed by two ground-state and one excited-state sublevels coupled by the pump and probe fields. Notice that when $\Delta \neq 0$ as in Figs. 5(c,d) the feature at $\delta=0$ becomes asymmetric. For $\Omega_1 \approx \Gamma$ narrow absorption and gain peaks appear on either side of this structure. From simple three-level (Λ scheme) models, one can predict that when Ω_1 is increased, the narrow EIT structure at $\delta=0$ will continuously broaden and transform into the Autler-Townes doublet. The calculated spectra shown in Figs. 5(c,d) follow this pattern. In agreement with our simple considerations above, for large Ω_1 the spectra consist of one (d) or two (c) Autler-Townes absorption doublets.

The spectra corresponding to the $F_g=2 \rightarrow F_e=2$ transition are shown in Figs. 6 and 7 for $\Delta=0$ and $\Delta=2\Gamma$, re-

TABLE II. Values of $\delta \equiv \omega_2-\omega_1$ corresponding to the positions of the spectral features in the probe absorption spectra of strongly driven degenerate two-level atoms for different transitions and pump and probe polarizations linear and parallel (ll), linear and perpendicular (lpl), circular and equal (cc), and circular and opposite (coc). D_q^p is a compact notation for $D_q^p(F_g,F_e)=\frac{1}{2}\sqrt{\Delta^2+\Omega_1^2 C_q^p(F_g,F_e)^2}$ where $C_p^q(F_g,F_e)=\binom{F_g \quad F_e \quad 1}{q \quad -(p+q) \quad p}$ is a $3J$ coefficient.

cc	ll	coc	lpl
$F \rightarrow F-1$		$-\Delta/2 \pm D^1_{F-2}, -\Delta/2 \pm D^1_{F-3}$	$-\Delta/2 \pm D^0_{F-1}$
$F \rightarrow F$		$-\Delta/2 \pm D^1_{F-2}$	$-\Delta/2 \pm D^0_1$
$F \rightarrow F+1$	$0, \pm D^1_F$ $0, \pm D^0_m$ $(0 \leq m \leq F)$	$\pm D^1_{F-2} \pm D^1_F$	$\Delta/2 \pm D^0_F, \pm D^0_m \pm D^0_{m+1}$ $(0 \leq m < F)$

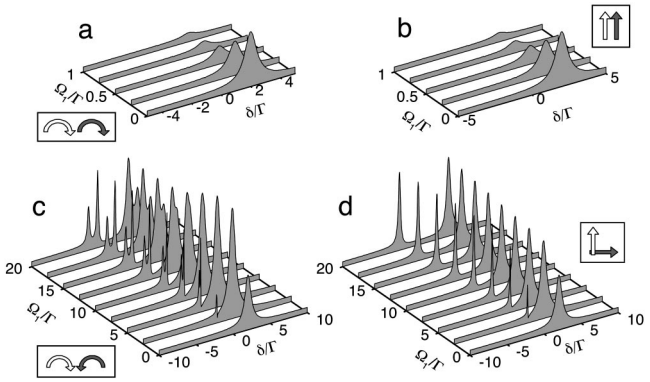

FIG. 5. Calculated probe absorption spectra for the transition $F_g=2\rightarrow F_e=1$ as a function of the probe frequency offset δ for different values of Ω_1 and $\Delta=2\Gamma$. Same conventions as in Fig. 4.

spectively. Their characteristics are very similar to those obtained for the $F_g=2\rightarrow F_e=1$ transition, except for the fact that the coc polarization case gives rise to a single Autler-Townes absorption doublet.

The most interesting case corresponds to the transition $F_g=1\rightarrow F_e=2$ presented in Figs. 8 and 9. For large values of Ω_1, the main elements of the absorption spectra are in agreement with the simple predictions presented in Tables I and II: one MAS (cc), two MAS's with a common central feature (ll), four absorption peaks (coc), and a six-peak structure (lpl). However, additional characteristics of the spectrum can now be appreciated. As Ω_1 is increased, the spectra corresponding to the cc case approaches the classical Mollow result [22] but for moderate values of the Rabi frequency ($\Omega_1\sim\Gamma$) there is an increase of the absorption peak not present in PTLS's. It is due to the optical pumping of the ground-state population into a Zeeman sublevel with the highest $|m|$. The lpl polarization combinations presents a richer spectral variation. For $\Omega_1\lesssim\Gamma$ (not presented in the figure) and $\Delta<\Gamma$ a large and narrow absorption enhancement (above linear absorption) appears at $\delta=0$ [13]. This corresponds to the effect of electromagnetically induced absorption (EIA) [12–14]. For $\Delta>\Gamma$ the EIA peak evolves into a narrow dispersionlike structure with absorption and gain

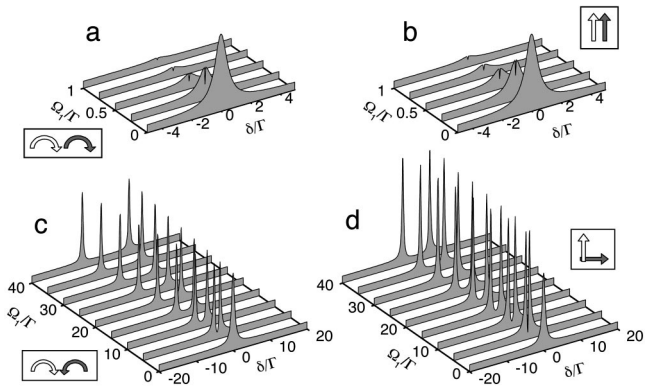

FIG. 6. Calculated probe absorption spectra for the transition $F_g=2\rightarrow F_e=2$ as a function of the probe frequency offset δ for different values of Ω_1 and $\Delta=0$. Same conventions as in Fig. 4.

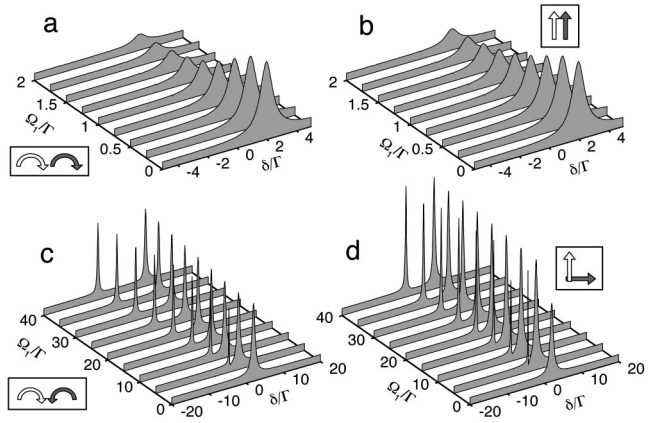

FIG. 7. Calculated probe absorption spectra for the transition $F_g=2\rightarrow F_e=2$ as a function of the probe frequency offset δ for different values of Ω_1 and $\Delta=2\Gamma$. Same conventions as in Fig. 4.

[Fig. 9(d)]. This structure differs from the central structure of the MAS in several aspects: (1) It is narrower; the width of the absorption and gain peaks are significantly smaller than Γ even for relatively large values of Ω_1 ($\Omega_1\gtrsim 10\Gamma$, see Fig. 19 in the Appendix). In contrast the width of the central dispersive feature of the MAS is determined by Γ. (2) It has the opposite symmetry than the central feature in the MAS. (3) Much larger values of the absorption and gain peaks compared to the main absorption resonance are attained. (4) At high pump intensities the dispersionlike structure evolves into two absorption peaks.

Some resonances appearing in the spectra presented in Fig. 9(d) change sign as Ω_1 is increased. This behavior can be explained with the help of dressed-state theory applied to the multilevel structure corresponding to this case. This analysis is presented in the Appendix.

The numerically calculated spectra provide a detailed insight into the shape and width of the different resonances. Some absorption or gain peaks appear to be narrower than the excited-state width Γ. These peaks are associated with Raman processes starting and ending in the ground level and involving one photon of each of the pump and probe fields.

The previous results concern a few basic schemes of optical polarization. An interesting feature of DTLS absorption

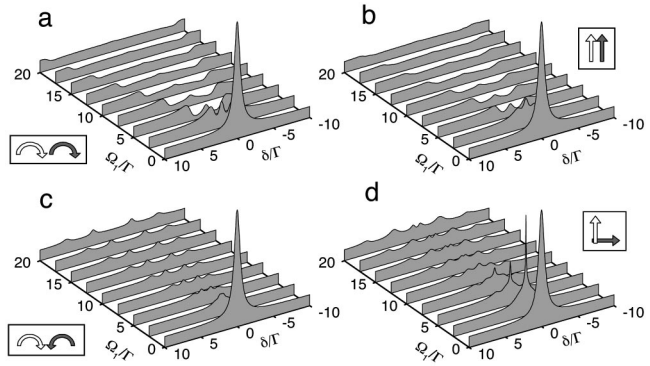

FIG. 8. Calculated probe absorption spectra for the transition $F_g=1\rightarrow F_e=2$ as a function of the probe frequency offset δ for different values of Ω_1 and $\Delta=0$. Same conventions as in Fig. 4.

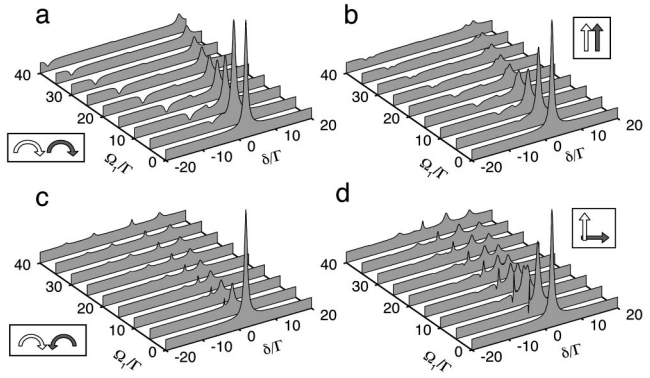

FIG. 9. Calculated probe absorption spectra for the transition $F_g=1\rightarrow F_e=2$ as a function of the probe frequency offset δ for different values of Ω_1 and $\Delta=2\Gamma$. Same conventions as in Fig. 4.

spectra appears to be the variation of the number of resonances with the choice of the optical polarization. For some polarizations the number of resonances is fixed and independent of F while for other combinations the number of resonances is a function of F. Since our model is able to handle arbitrary polarizations we have explored intermediate situations between these cases. Figures 10 and 11 show the modification in the absorption spectra for a continuous variation of the polarization from lpl to coc and ll to cc, respectively, by gradually varying the ellipticity of the field polarization. These two cases have been chosen since they can be explored experimentally using copropagating linearly polarized pump and probe fields passing through a rotatable quarter-wave plate. As can be appreciated in Fig. 10 the absorption spectrum is rather rich for orthogonal elliptical polarizations (up to 13 peaks are present in this figure for an ellipticity around 0.7).

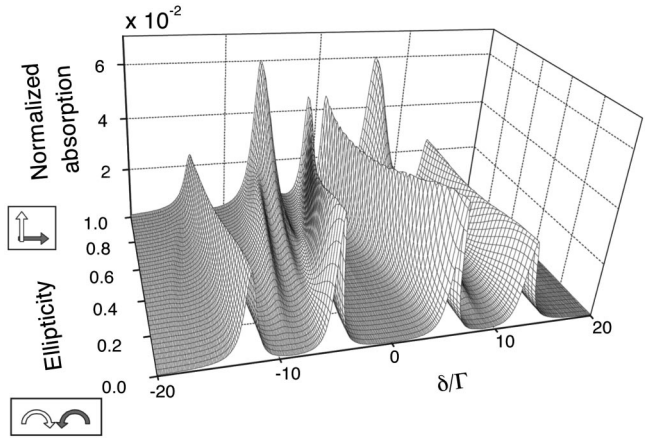

FIG. 10. Calculated probe absorption spectra for the transition $F_g=1\rightarrow F_e=2$ as a function of δ for $\Omega_1=40\Gamma$ and $\Delta=0$ for different values of the polarization ellipticity $1-\xi$ $(0\leqslant\xi\leqslant1)$. The pump and probe polarization vectors are given by $\mathbf{e}_1=\cos(\pi\xi/4)\mathbf{e}_x+i\sin(\pi\xi/4)\mathbf{e}_y$ and $\mathbf{e}_2=i\sin(\pi\xi/4)\mathbf{e}_x+\cos(\pi\xi/4)\mathbf{e}_y$ ($\mathbf{e}_x$ and $\mathbf{e}_y$ are unit vectors along the coordinate axes). The absorption is normalized to the linear absorption.

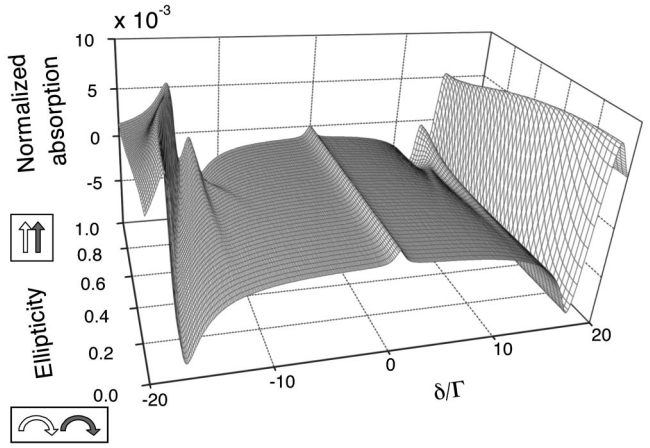

FIG. 11. Calculated probe absorption spectra for the transition $F_g=1\rightarrow F_e=2$ as a function of δ for $\Omega_1=40\Gamma$ and $\Delta=0$ for different values of the polarization ellipticity $1-\xi$ $(0\leqslant\xi\leqslant1)$. The pump and probe polarizations vectors are equal and given by $\mathbf{e}=\cos(\pi\xi/4)\mathbf{e}_x+i\sin(\pi\xi/4)\mathbf{e}_y$ ($\mathbf{e}_x$ and $\mathbf{e}_y$ are unit vectors along the coordinate axes). The absorption is normalized to the linear absorption.

III. EXPERIMENT

The experimental observations of driven DTLS absorption spectra were carried on the $5S_{1/2}(F=3)\rightarrow5P_{3/2}(F=4)$ transition of ^{85}Rb. This transition corresponds to the case (ii) discussed above for which the richer spectra occur. To reduce Doppler broadening, we used a rubidium atomic beam. The Rb reservoir was heated to approximately 200 °C. The atoms exit the reservoir through multiple 0.5 mm internal diameter and 5 mm long tubes forming an 8 mm diameter output nozzle. 30 cm downstream the atoms are collimated by a rectangular slit 1 mm high and 10 mm wide. The atoms are illuminated 6 cm after the slit. The light beams exciting the atoms propagate in the same direction parallel to the longest collimating slit dimension. The linear absorption in

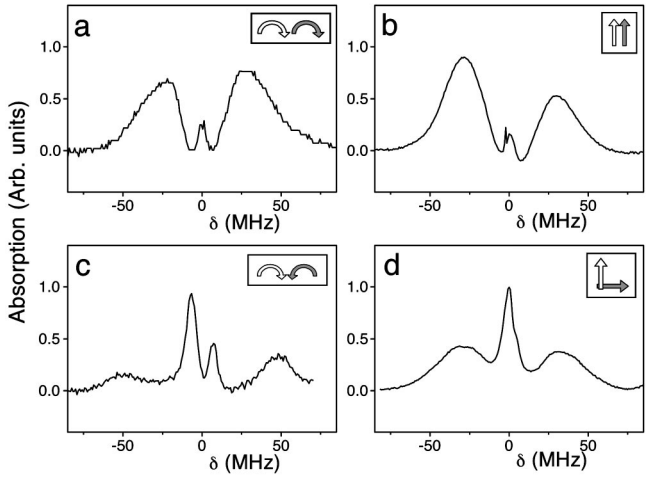

FIG. 12. Observed absorption spectra for the driven $5S_{1/2}(F=3)\rightarrow5P_{3/2}(F=4)$ transition of ^{85}Rb for $\Delta=0$. The pump and probe polarizations are circular and equal (a), linear and parallel (b), circular and opposite (c), and linear and perpendicular (d).

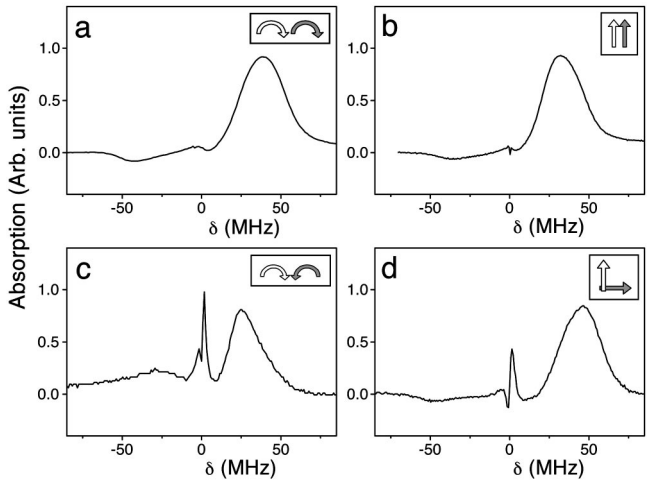

FIG. 13. Observed absorption spectra for the driven $5S_{1/2}(F=3)\rightarrow 5P_{3/2}(F=4)$ transition of ^{85}Rb for $\Delta \geqslant \Gamma = 6$ MHz. The polarization cases are those of Fig. 12. (a) $\Delta = 24$ MHz. (b) $\Delta = 23$ MHz. (c) $\Delta = 6$ MHz. (d) $\Delta = 22$ MHz.

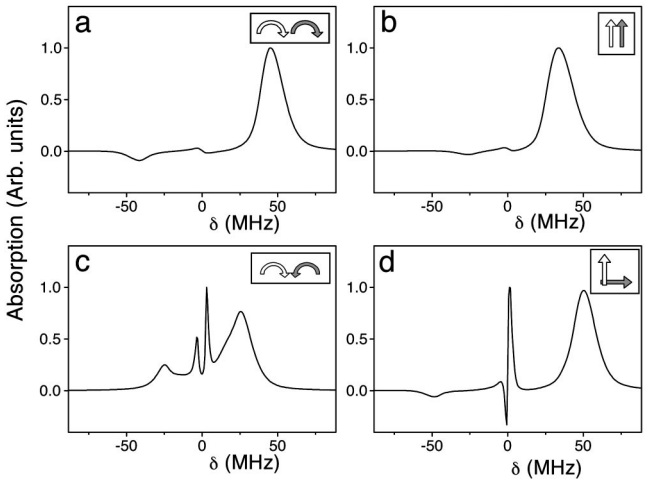

FIG. 15. Calculated absorption spectra for the transition $F_g=3 \rightarrow F_e=4$ for the cases considered in Fig. 13 for conditions corresponding to the experiment (see text). (a) $\Omega_1 = 9.5\Gamma$. (b) $\Omega_1 = 6\Gamma$. (c) $\Omega_1 = 8\Gamma$. (d) $\Omega_1 = 12\Gamma$.

the studied transition was approximately 8%. The residual Doppler width of the transition was 24 MHz [full width at half maximum (FWHM)]. The atomic beam apparatus was continuously pumped to less than 10^{-6} Torr. To help maintain the vacuum and reduce the rubidium vapor background, a liquid nitrogen cooled trap was connected to the atomic beam chamber. The pump and probe fields were obtained from two independent extended cavity diode lasers (linewidth ~ 1 MHz). The pump laser frequency was fixed close to the $5S_{1/2}(F=3)\rightarrow 5P_{3/2}(F=4)$ transition. The pump laser frequency drift during the measurements was less than 2 MHz. The probe laser frequency was scanned around the studied transition. The pump and probe beam diameters in the interaction zone were approximately 2 mm and 1 mm and their typical powers 5 mW and 2 μW, respectively. The polarizations of the two beams were independently controlled. The two beams were incident at right angles with respect to the atomic beam. A small angle (5 mrad) was introduced between the two beams to allow separate detection. After interacting with the atoms, the probe beam intensity was measured with a photodiode whose output was directly monitored on an oscilloscope. A fraction of the probe laser output was sent to a saturated absorption setup using a Rb vapor cell. Both the probe absorption spectrum on the atomic beam and the saturated absorption spectrum on the vapor cell were recorded simultaneously for frequency calibration. The detuning Δ was determined with a precision of

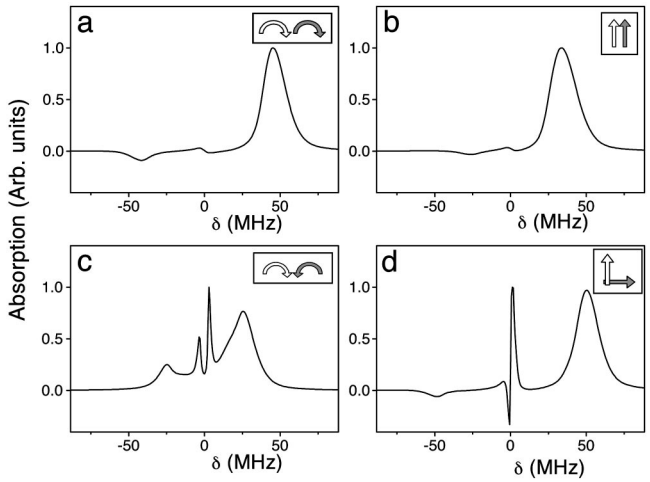

FIG. 14. Calculated absorption spectra for the transition $F_g=3 \rightarrow F_e=4$ for the polarization cases considered in Fig. 12 for conditions corresponding to the experiment (see text). $\Omega_1 = 5\Gamma$ (a,b,d). $\Omega_1 = 15\Gamma$ (c).

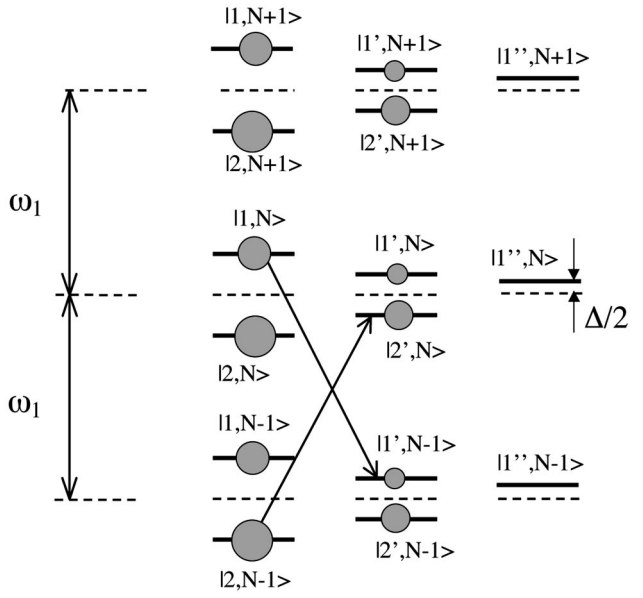

FIG. 16. Schematic representation of the dressed-state level diagram corresponding to the transition $F_g=1\rightarrow F_e=2$ with linear and perpendicular pump probe polarizations. Only ladders corresponding to $m \geqslant 0$ are presented. $\Delta > 0$ is assumed. Circles represent occupation numbers. The arrows indicate two transitions contributing to the same absorption line.

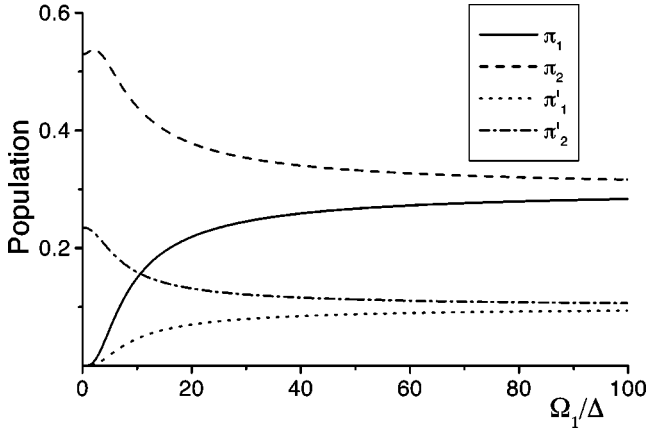

FIG. 17. Steady state occupation numbers π_1, π_2, π_1', π_2' corresponding to the dressed states $|1,N\rangle$, $|2,N\rangle$, $|1',N\rangle$, $|2',N\rangle$, respectively, as a function of Ω_1/Δ.

± 2 MHz. The magnetic field in the interaction region was not compensated (<120 mG). However, its influence is expected to be small for the experimental conditions considered.

We have investigated the cc, coc, ll, and lpl pump and probe polarization cases. The corresponding spectra are presented in Figs. 12 and 13 for zero ($\Delta=0\pm 2$ MHz) and nonzero ($|\Delta|\geqslant\Gamma=6$ MHz) pump field detuning, respectively.

The experimental spectra show a qualitative agreement with the spectra calculated for the simpler $F_g=1\rightarrow F_e=2$ transition for Ω_1 in the range $2\Gamma\leqslant\Omega_1\leqslant 10\Gamma$ (Figs. 8 and 9) . The main features in the calculated spectra are present in the experimental curves. Not surprisingly, the spectrum for the cc configuration approaches the MAS [22]. The ll experimental spectra are consistent with several (unresolved) MAS's. The coc case gives rise to a four-absorption-peak structure with different linewidths. Finally, the lpl case shows a relatively narrow central absorption peak for $\Delta=0$ and an asymmetric narrow feature with absorption and gain when $\Delta>\Gamma$.

A more precise comparison of the experimental spectra with the theoretical predictions requires consideration of the

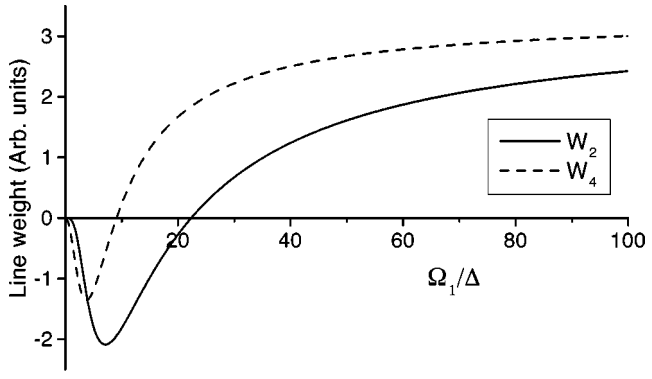

FIG. 18. Line weights W_2 and W_4 of the peaks presenting sign changes in the absorption spectrum as a function of Ω_1/Δ. Negative values indicate gain.

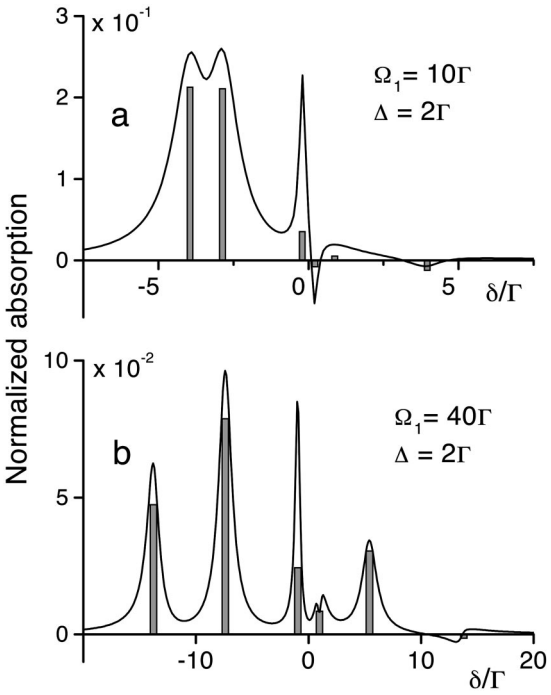

FIG. 19. Dressed-state absorption ''spectra'' (bars) for the transition $F_g=1\rightarrow F_e=2$ for $\Omega_1=10\Gamma$ (a) and $\Omega_1=40\Gamma$ (b) with $\Delta=2\Gamma$. The bar height represents the weight (arbitrary units) of a given peak. Solid lines: calculated absorption spectra according to our model (normalized to the linear absorption).

main differences between the actual experimental conditions and the assumptions of the theory. These result from two practical aspects that limit the homogeneous nature of the atomic sample: the residual transverse velocity distribution of the atoms in the beam and the spatial variation of the pump laser intensity (and thus the Rabi frequency) in the interaction region. Figures 14 and 15 show the absorption spectra calculated with our model for parameters corresponding to the experimental conditions. In these calculations the Rabi frequency Ω_1 was used as an adjustable parameter. The effect of the residual Doppler broadening was taken into consideration by averaging the probe absorption spectra over a Gaussian distribution for the detuning Δ with 24 MHz width (FWHM). We used as the central value of the Δ distribution $\Delta=0$ for Fig. 14 and the measured detunings of the pump frequency with respect to the $5S_{1/2}(F=3)\rightarrow 5P_{3/2}(F=4)$ transition for Fig. 15. We did not attempt to include in the calculation the effect of the spatial variation of the pump intensity.

The agreement between the calculated and observed spectra is satisfactory. The larger width of some experimentally observed features with respect to the calculations is probably the consequence of the spatial inhomogeneity of the pump intensity. Each of the polarization cases presents a rather characteristic spectrum. The predictions concerning the sign of the resonances (absorption or gain) are verified. Finally, the experimental spectra confirm the theoretical predictions concerning the differences in the linewidth. Of particular interest is the rather narrow sign-changing structure observed in the lpl polarization case. This structure reproduces the

main features predicted by Bo Gao [19] and by our calculation. It bears a clear resemblance to the structure observed in the probe spectra of magneto-optically trapped atoms [10,11] although in this case, additional effects due to the spatial distributions of the Rabi frequency, the polarization, and the magnetic field may influence the absorption spectra.

IV. CONCLUSIONS

We have addressed the problem of the absorption spectra of a closed system formed by two degenerate atomic levels, with well defined angular momentum, driven by a pump field. A theoretical model, previously presented in [14], was used to calculate the absorption spectra for arbitrary choices of the atomic transition, the pump field intensity, and the pump and probe polarizations. As a representative example, the spectra corresponding to different choices of the optical polarizations were calculated for the simple $2\rightarrow1$, $2\rightarrow2$, and $1\rightarrow2$ transitions. In contrast with the classical pure two-level system case studied by Mollow and co-workers, a large variety of spectra were predicted and the characteristic features identified and discussed. The experimentally observed probe absorption spectra on a beam of ^{85}Rb atoms driven on the $5S_{1/2}(F=3)\rightarrow5P_{3/2}(F=4)$ transition show good agreement with the predictions of our model.

ACKNOWLEDGMENTS

The authors are grateful to R. San Vicente and L. Barboni for their help in the construction of the atomic beam apparatus. This work was supported by the Uruguayan agencies CONICYT, CSIC, and PEDECIBA, and by the ICTP/CLAF.

APPENDIX: DRESSED-STATES TREATMENT OF A DTLS WITH LINEAR PERPENDICULAR PUMP AND PROBE POLARIZATIONS

The dressed-states treatment [20] of a DTLS with lpl pump and probe polarizations provides an interesting insight into the peculiarities observed in the probe absorption spectrum in this case. In particular, it provides a simple explanation for the sign change observed for some peaks as Ω_1 is increased. Here we will briefly develop this treatment [26] and compare its results with those arising from the model discussed above.

We consider again as an example the $F_g=1\rightarrow F_e=2$ transition which is the simplest interesting case. The quantization axis is chosen to coincide with the pump polarization direction. In consequence, the pump field couple atomic states with the same m. Figure 16 shows a schematic representation of the level structure resulting from the coupling of the atomic system and pump photons. In this figure, the $m\leftrightarrow-m$ symmetry was used to simplify the diagram: a single ladder is used to represent states involving the same $|m|$. Circles indicate stationary populations.

The dressed-state properties depend on the two parameters θ and θ' given by

$$\tan(2\theta)=C_0\frac{\Omega_1}{\Delta}\quad(0\leqslant\theta\leqslant\pi/2),\tag{A1}$$

$$\tan(2\theta')=C_1\frac{\Omega_1}{\Delta}\quad(0\leqslant\theta'\leqslant\pi/2),\tag{A2}$$

where $C_m\equiv\left(\begin{smallmatrix}1&2&1\\m&-m&0\end{smallmatrix}\right)$ is a $3J$ coefficient.

The dressed states represented in Fig. 16 are thus given by

$$\begin{aligned}
|1,N\rangle&=\sin(\theta)|g,0\rangle|N+1\rangle+\cos(\theta)|e,0\rangle|N\rangle,\\
|2,N\rangle&=\cos(\theta)|g,0\rangle|N+1\rangle-\sin(\theta)|e,0\rangle|N\rangle,\\
|1',N\rangle&=\sin(\theta')|g,1\rangle|N+1\rangle+\cos(\theta')|e,1\rangle|N\rangle,\\
|2',N\rangle&=\cos(\theta')|g,1\rangle|N+1\rangle-\sin(\theta')|e,1\rangle|N\rangle,\\
|1'',N\rangle&=|e,2\rangle|N\rangle,
\end{aligned}\tag{A3}$$

where $|g,m\rangle$ and $|e,m\rangle$ represent atomic states in the ground and excited levels, respectively, with magnetic quantum number m. $|N\rangle$ denotes a pump field photon number state. The last state in Eqs. (A3) is an uncoupled atom-photon state.

The steady state occupation numbers (populations) π_1, π_2, π_1', π_2', and π_1'' corresponding respectively to the states defined in Eq. (A3) can be computed by solving a set of rate equations describing the radiative cascade due to spontaneous emission [20]. Notice that in this case the radiative decay transfers population between the different ladders.

The result of this calculation is presented in Fig. 17 as a function of Ω_1/Δ. Also, $\pi_1''=0$. Notice the change in the sign of $\pi_1-\pi_2'$ occurring for $\Omega_1/\Delta\simeq10$.

The weights of the different lines composing the absorption spectrum (whose positions are indicated in Table II) can be computed using first order perturbation theory and the occupation numbers of the different levels. They are given by

$$\begin{aligned}
W_1&=2[(\pi_2-\pi_1')d_{01}^2+(\pi_2'-\pi_1)d_{10}^2]\cos^2(\theta)\cos^2(\theta'),\\
W_2&=2[(\pi_1-\pi_2')d_{01}^2+(\pi_1'-\pi_2)d_{10}^2]\sin^2(\theta)\sin^2(\theta'),\\
W_3&=2[(\pi_2-\pi_2')d_{01}^2+(\pi_1'-\pi_1)d_{10}^2]\cos^2(\theta)\sin^2(\theta'),\\
W_4&=2[(\pi_1-\pi_1')d_{01}^2+(\pi_2'-\pi_2)d_{10}^2]\sin^2(\theta)\cos^2(\theta'),\\
W_5&=2\pi_1'd_{12}^2\sin^2(\theta'),\\
W_6&=2\pi_2'd_{12}^2\cos^2(\theta'),
\end{aligned}\tag{A4}$$

where $d_{mn}\equiv\langle g,m|D|e,n\rangle$ is a matrix element of the electric dipole between a ground- and an excited-state sublevel.

Examination of Eqs. (A4) and the computed populations (Fig. 17) shows that W_1, W_3, W_5, and W_6 always correspond to absorption peaks while W_2 and W_4 present a vari-

able sign depending on the distribution of populations. Figure 18 presents the variation of these two weights as a function of Ω_1/Δ. Both lines correspond to gain for small values of Ω_1/Δ and evolve into absorption peaks for large Ω_1/Δ.

Finally, Fig. 19 shows the weights of the absorption spectral lines deduced from the dressed-state model for two different values of Ω_1. For comparison, the calculated spectra provided by our model are also presented.

[1] L. Allen and J.H. Eberly, *Optical Resonance and Two-Level Atoms* (Wiley, New York, 1975).

[2] Y. R. Shen, *The Principles of Nonlinear Optics* (Wiley, New York, 1984).

[3] B. R. Mollow, Phys. Rev. A **3**, 2217 (1972).

[4] F. Y. Wu, S. Ezekiel, M. Ducloy, and B. R. Mollow, Phys. Rev. Lett. **38**, 1077 (1977).

[5] B. R. Mollow, Phys. Rev. **188**, 1969 (1969); R. E. Grove, F. Y. Wu, and S. Ezekiel, Phys. Rev. A **15**, 227 (1977).

[6] C. Cohen-Tannoudji and S. Haroche, J. Phys. (Paris) **30**, 125 (1969); C. Cohen-Tannoudji and S. Reynaud, J. Phys. B **10**, 345 (1977); C. Cohen-Tannoudji, in *Frontiers in Laser Spectroscopy*, edited by R. Balian, S. Haroche, and S. Liberman (North-Holland, Amsterdam, 1977), Vol. 1, and references therein.

[7] E. L. Raab, M. Prentiss, A. Cable, S. Chu, and D. E. Pritchard, Phys. Rev. Lett. **59**, 2631 (1987).

[8] J. Dalibard and C. Cohen-Tannoudji, J. Opt. Soc. Am. B **6**, 2023 (1989).

[9] A. Aspect, E. Arimondo, R. Kaiser, N. Vansteenkiste, and C. Cohen-Tannoudji, Phys. Rev. Lett. **61**, 826 (1988).

[10] J. W. R. Tabosa, G. Chen, Z. Hu, R. B. Lee, and H. J. Kimble, Phys. Rev. Lett. **66**, 3245 (1991).

[11] D. Grison, B. Lounis, C. Salomon, Y. J. Courtois, and G. Grynberg, Europhys. Lett. **15**, 149 (1991).

[12] A. M. Akulshin, S. Barreiro, and A. Lezama, Phys. Rev. A **57**, 2996 (1998).

[13] A. Lezama, S. Barreiro, and A. M. Akulshin, Phys. Rev. A **59**, 4732 (1999).

[14] A. Lezama, S. Barreiro, A. Lipsich, and A. M. Akulshin, Phys. Rev. A **61**, 013801 (1999).

[15] C. Feuillade and P. R. Berman, Phys. Rev. A **29**, 1236 (1984).

[16] P. R. Berman, D. G. Steel, G. Khitrova, and J. Liu, Phys. Rev. A **38**, 252 (1988).

[17] P. R. Berman, Phys. Rev. A **43**, 1470 (1991).

[18] Bo Gao, Phys. Rev. A **48**, 2443 (1993).

[19] Bo Gao, Phys. Rev. A **49**, 3391 (1994).

[20] C. Cohen-Tannoudji, J. Dupont-Roc, and G. Grynberg, *Atom-Photon Interactions* (Wiley, New York, 1992).

[21] G. Grynberg and C. Cohen-Tannoudji, Opt. Commun. **96**, 150 (1993).

[22] The same polarization configuration was used by Wu and coworkers (Ref. [4]) for the experimental observation of the MAS.

[23] E. V. Baklanov and V. P. Chebotaev, Zh. Éksp. Teor. Fiz. **61**, 922 (1971) [Sov. Phys. JETP **34**, 490 (1972)].

[24] S. Haroche and F. Hartmann, Phys. Rev. A **6**, 1280 (1972).

[25] A. Wilson-Gordon and H. Friedmann, Opt. Lett. **14**, 390 (1989).

[26] C. Cohen-Tannoudji and S. Reynaud, J. Phys. (Paris) **38**, L173 (1977).